Acta Crystallographica Section F
Structural Biology and Crystallization Communications
ISSN 1744-3091

Crystallization of the *Staphylococcus aureus* MazF mRNA interferase

Valentina Zorzini,[a,b] Sarah Haesaerts,[a,b] Niles P. Donegan,[c] Zhibiao Fu,[c] Ambrose L. Cheung,[c] Nico A. J. van Nuland[a,b] and Remy Loris[a,b]*

[a]Structural Biology Brussels, Vrije Universiteit Brussel, Pleinlaan 2, B-1050 Brussel, Belgium, [b]Department of Molecular and Cellular Interactions, Vrije Universiteit Brussel, Pleinlaan 2, B-1050 Brussel, Belgium, and [c]Department of Microbiology and Immunology, Dartmouth Medical School, Hanover, NH 03755, USA

Correspondence e-mail: reloris@vub.ac.be

Received 16 November 2010
Accepted 5 January 2011

mazEF modules encode toxin–antitoxin pairs that are involved in the bacterial stress response through controlled and specific degradation of mRNA. *Staphylococcus aureus* MazF and MazE constitute a unique toxin–antitoxin module under regulation of the *sigB* operon. A MazF-type mRNA interferase is combined with an antitoxin of unknown fold. Crystals of *S. aureus* MazF (*Sa*MazF) were grown in space group $P2_12_12_1$. The crystals diffracted to 2.1 Å resolution and are likely to contain two *Sa*MazF dimers in the asymmetric unit.

1. Introduction

Toxin–antitoxin (TA) modules are small operons encoding a growth inhibitor (the 'toxin') and a protein (the 'antitoxin') that regulates the activity of the toxin by direct inhibition and by acting as a transcription regulator (Buts *et al.*, 2005; Gerdes *et al.*, 2005). TA modules were initially discovered as 'plasmid addiction modules' on low-copy-number plasmids such as F or R1 and on plasmidic phages such as P1 (Ogura & Hiraga, 1983; Bravo *et al.*, 1987; Lehnherr *et al.*, 1993). They ensure plasmid maintenance by a mechanism of post-segregational killing that relies on a difference in the lifetime of the toxin and the antitoxin (Gerdes *et al.*, 1986). However, most TA modules are encoded on chromosomes and their functional role is a matter of heavy debate. A number of different functions have been proposed, ranging from selfish genes through stabilization of specific chromosomal segments to roles in stress response and persister-cell formation (Magnuson, 2007; Van Melderen, 2010).

The *mazEF* family of TA modules constitutes one of the larger TA families and is found on chromosomes of both Gram-negative and Gram-positive bacteria (but not in archaea; Pandey & Gerdes, 2005). The toxin MazF is a ribonuclease that cuts mRNA at highly specific sites (Zhang *et al.*, 2003), leading to a redirection of translation towards the synthesis of a few specific proteins (Amitai *et al.*, 2009; Baik *et al.*, 2009). Different family members show different cutting specificities which relate to the specific cellular functions of individual MazF-family members (Yamaguchi & Inouye, 2009). This property has been used to create a single protein-production system (Suzuki *et al.*, 2005). In contrast to RelE (the mRNA-cleavage enzyme from the RelBE TA pair), mRNA cleavage by MazF generally occurs independently of translation, although for some specific RNAs translation significantly influences the observed cleavage rates (Christensen-Dalsgaard & Gerdes, 2008). Long-term activation of MazF leads to cell death, and MazF activation within an *Escherichia coli* population has been linked to quorum sensing (Amitai *et al.*, 2004; Kolodkin-Gal *et al.*, 2007).

While *mazEF* modules from Gram-negative bacteria, and especially *E. coli* and *Mycobacterium tuberculosis*, have been heavily studied (Inouye, 2006), less is known about *mazEF* modules in Gram-positive bacteria. The genome of *Staphylococcus aureus* contains a single *mazEF* module that is highly conserved in all *Staphylococcus* species, including MRSA and VRSA strains (Fu *et al.*, 2007). In

contrast to the typical situation in Gram-negative bacteria, the *S. aureus mazEF* module (*SamazEF*) does not form an isolated operon but belongs to the *sigB* operon that encodes the σ^{B} sigma factor and its control genes *rsbU*, *rsbV* and *rsbW* (Donegan & Cheung, 2009). *Sa*MazE and *Sa*MazF are co-transcribed with these four genes. While the *SamazF* gene encodes a protein that is weakly related to *E. coli* MazF (16% sequence identity), the 56-amino-acid *Sa*MazE protein shows no detectable sequence identity to MazE proteins from Gram-negative bacteria. *Sa*MazF was shown to cleave mRNA *in vitro*, although there is discussion about its sequence specificity (Fu *et al.*, 2007; Zhu *et al.*, 2009). Here, we present the crystallization and preliminary X-ray analysis of *Sa*MazF.

2. Material and methods

2.1. Protein production

The *SamazE* (SACOL2059; UniProtKB entry Q5HED2) and *SamazF* (SACOL2058; UniProtKB entry Q5HED3) genes were cloned into pDuet1 as described previously (Fu *et al.*, 2007), placing a His tag at the N-terminus of the *Sa*MazF protein. The vector was transformed into *E. coli* BL21 (DE3) cells using the $CaCl_2$ method. A 25 ml overnight preculture in LB medium supplemented with 100 µg ml^{-1} ampicillin was used to inoculate (1:100 dilution) 1 l LB medium supplemented with the same concentration of ampicillin and 0.2%(*w*/*v*) glucose. When the culture reached an OD_{600} of 0.6, expression of the proteins was induced by adding 1 m*M* isopropyl *β*-D-1-thiogalactopyranoside (IPTG). The induced culture was further incubated overnight at 310 K while stirring at 120 rev min^{-1}. The cells were harvested by centrifugation (25 min at 11 000*g* using a Beckman JLA 8.1000 rotor at 5500 rev min^{-1}) and the pellet was resuspended in 50 ml lysis buffer (100 m*M* Tris–HCl pH 8.0, 1 *M* NaCl, 20 m*M* imidazole, 0.1 mg ml^{-1} AESBF and 1 µg ml^{-1} leupeptin). The suspension was then passed twice through a French press and centrifuged at 43 500*g* for 30 min (using a Beckman JA-20 rotor at 18 000 rev min^{-1}). The supernatant was filtered through a 0.45 µm Sartorius Minisart filter and loaded onto a pre-packed 1 ml Ni–NTA column (Qiagen) equilibrated in 50 m*M* Tris–HCl pH 7.0, 250 m*M* NaCl (washing buffer). The column was then washed with ten column volumes of washing buffer prior to elution with a gradient of 0–1 *M* imidazole in 50 m*M* Tris–HCl pH 7.0, 250 m*M* NaCl. The *Sa*MazE–*Sa*MazF complex thus obtained was dialyzed against 50 m*M* Tris–HCl pH 7.0, 250 m*M* NaCl and concentrated using a Vivaspin concentrator (10 000 Da molecular-weight cutoff). *Sa*MazF and *Sa*MazE were obtained by unfolding and refolding as described previously (Fu *et al.*, 2007). The purity of the proteins was evaluated using SDS–PAGE.

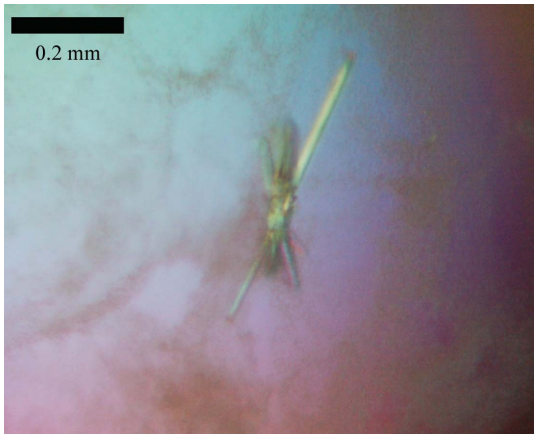

Figure 1
Typical crystals of *Sa*MazF.

Table 1
Data-collection and processing statistics.

Values in parentheses are for the highest resolution shell.

No. of crystals	1
Beamline	PROXIMA1
Wavelength (Å)	1.0394
Detector	ADSC Q315r
Crystal-to-detector distance (mm)	300
Rotation range per image (°)	1.0
Total rotation range (°)	150
Exposure time per image (s)	1.0
Resolution range (Å)	56.34–2.10 (2.16–2.10)
Space group	$P2_12_12_1$
Unit-cell parameters (Å)	a = 60.72, b = 65.36, c = 112.01
Mosaicity (°)	0.21–0.61
Total no. of measured intensities	144316 (9030)
Unique reflections	26598 (2150)
Multiplicity	5.4 (4.2)
Mean $I/\sigma(I)$	14.0 (3.4)
Completeness (%)	99.8 (98.8)
R_{merge}† (%)	10.4 (34.1)
Overall B factor from Wilson plot (Å^2)	30.3

† $R_{merge} = \sum_{hkl}\sum_i |I_i(hkl) - \langle I(hkl)\rangle| / \sum_{hkl}\sum_i I_i(hkl)$, where $I_i(hkl)$ is the ith observation of reflection hkl and $\langle I(hkl)\rangle$ is the weighted average intensity for all observations i of reflection hkl.

2.2. Crystallization

Protein samples (*Sa*MazE, *Sa*MazF and their complex) were dialyzed against a suitable buffer (50 m*M* Tris pH 7.0, 250 m*M* NaCl; 20 m*M* Tris pH 7.5, 150 m*M* NaCl; 20 m*M* sodium phosphate pH 6.6) and concentrated to 5–20 mg ml^{-1}. A complex between *Sa*MazF and a 33-amino-acid peptide corresponding to the C-terminus of *Sa*MazE (obtained from BioSynthesis, USA) was prepared under the same conditions by slowly adding a fivefold molar excess of the peptide to a concentrated *Sa*MazF solution followed by concentration. Crystallization conditions were screened using the hanging-drop vapour-diffusion method in 48-well plates with drops consisting of 2 µl protein solution and 2 µl reservoir solution equilibrated against 200 µl reservoir solution. Various commercial screens from Hampton Research were used for screening.

2.3. Data collection and analysis

An *Sa*MazF crystal was cryoprotected by direct transfer into the cryostream without the need for additional cryoprotectant. X-ray diffraction data were collected on the PROXIMA1 beamline at the SOLEIL synchrotron (Gif-Sur-Yvette, France) using a wavelength of 1.0394 Å. 150 useful images (out of 300) were collected on an ADSC Q315r CCD detector with a crystal-to-detector distance of 300 mm, 1.0° rotation per image and 1.0 s exposure time. A beam attenuation of 50% and a periodic translation of the crystal in the X-ray beam were used to minimize potential radiation damage. Data were indexed, integrated and scaled with *DENZO* and *SCALEPACK* from the *HKL*-2000 program package (Otwinowski & Minor, 1997). Analysis of the unit-cell contents was performed with the program *MATTHEWS_COEF* and self-rotation functions were calculated with *MOLREP*, both of which are part of the *CCP*4 package (Collaborative Computational Project, Number 4, 1994).

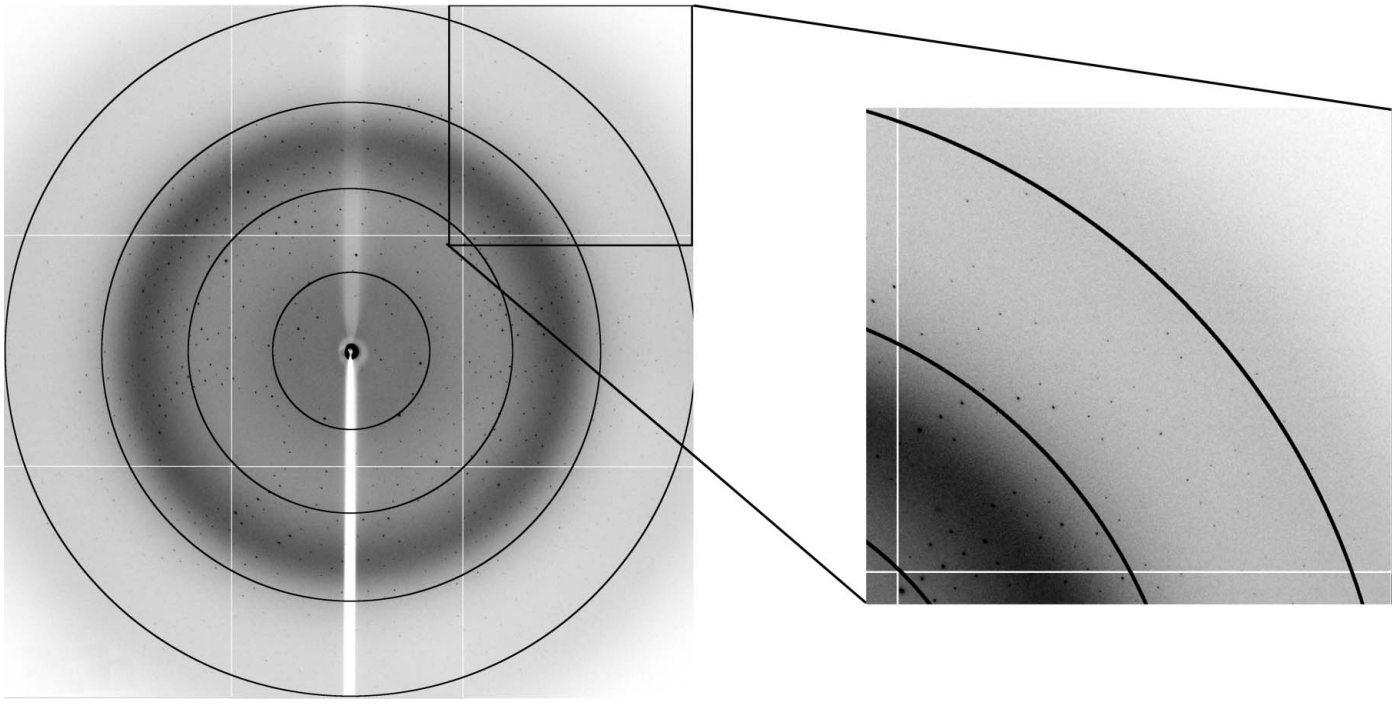

Figure 2
Diffraction pattern of a crystal of *Sa*MazF showing spots to 2.1 Å resolution. The image corresponds to 1.0 s exposure on the PROXIMA1 beamline of the SOLEIL synchrotron with the crystal rotated by 1°. Rings corresponding to resolutions of 8.7, 4.4, 2.9 and 2.2 Å are indicated. The inset shows an enlargement of the detector corner, showing spots to about 2.1 Å resolution.

3. Results and discussion

An *Sa*MazE–*Sa*MazF (*Sa*MazEF) complex was purified by Ni–NTA affinity chromatography and the individual *Sa*MazE and *Sa*MazF proteins were separated by treatment of the Ni–NTA-bound complex with GdHCl followed by refolding of *Sa*MazF on the column. Both *Sa*MazEF and *Sa*MazE formed large aggregates as assessed by DLS and analytical size-exclusion chromatography and attempts at crystallization failed (data not shown). *Sa*MazF, on the other hand, was monodisperse (2.1 nm, corresponding to a dimer, as is also the case for other MazF-family members) but still failed to crystallize in its free form. Screens set up with *Sa*MazF (20 m*M* Tris–HCl pH 7.5, 150 m*M* NaCl) in the presence of a fivefold excess of the C-terminal domain of *Sa*MazE (*Sa*MazE$^{23–56}$, residues Met23–Glu56) showed promising hits in a number of conditions. Well diffracting needle-shaped crystals were obtained in 0.2 *M* ammonium acetate, 0.1 *M* sodium acetate pH 4.6, 30%(*w*/*v*) polyethylene glycol 4000.

The crystals were needle-shaped and diffracted to about 2.1 Å resolution (Figs. 1 and 2). Despite their reasonable size (0.4 mm in their largest dimension) and the low X-ray dose used, they suffered from radiation damage during data collection. Therefore, a full data set required periodic translation of the crystal in the beam to expose fresh areas of the crystal. This involved three different areas of exposure, for each of which 100 images were collected. Only those images where radiation damage was not obvious (as monitored by the increase in *B* factor remaining below 5.0 Å^2 during scaling of the frames) were retained. This corresponds to 150 images, leading to a data set with an overall redundancy of 5.4. Full data-collection statistics are given in Table 1.

The unit-cell parameters were $a = 60.72$, $b = 65.36$, $c = 112.01$ Å and analysis of the systematic absences pinpointed the space group as $P2_12_12_1$. MazF proteins are known to be obligate dimers. Therefore, owing to crystal symmetry constraints the asymmetric unit can only contain one or more complete dimers. If it is assumed that each *Sa*MazF dimer has two *Sa*MazE$^{23–56}$ peptides bound, the resulting heterotetramer would have a molecular mass of 36 kDa. Matthews

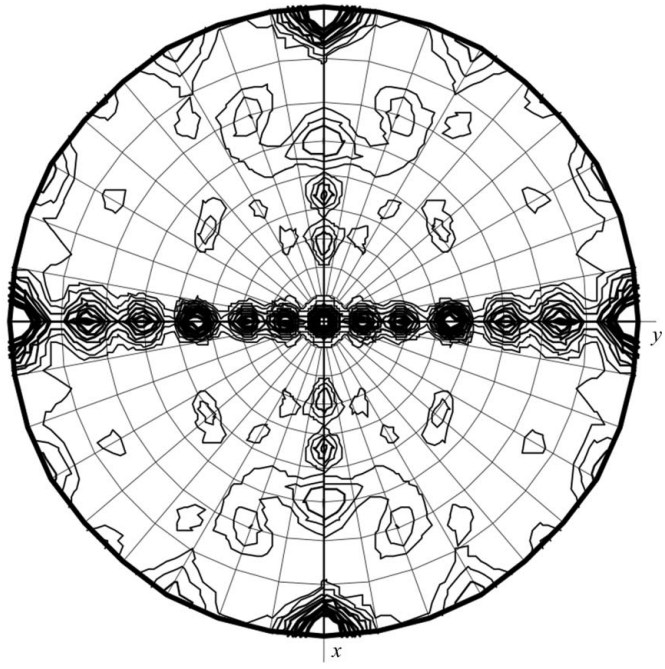

Figure 3
Self-rotation function showing the presence of several peaks on the $\kappa = 180°$ section. The self-rotation function was calculated using all data and a Patterson integration radius of 12 Å. Changing the resolution limits did not significantly affect the observed peaks, but their relative intensities varied when varying the integration radius between 8 and 14 Å.

analysis then points to a single heterotetramer being present in the asymmetric unit, corresponding to a solvent content of 59%. However, analysis of the self-rotation function indicated a more complex situation, with several significant peaks (Fig. 3). This indicates the presence of more than one dimer, which would only be possible if MazF crystallized without the MazE-derived peptide. Indeed, SDS–PAGE analysis of a washed crystal revealed only a single band corresponding to the size of *Sa*MazF. We thus conclude that the crystals are crystals of *Sa*MazF, although the *Sa*MazE-derived peptide apparently aided crystallization. It is possible that in the *SamazEF* system the C-terminus of the antitoxin may not be sufficient to recognize the toxin with high affinity as is the case for the *E. coli mazEF* module (Li *et al.*, 2006). The unit cell is likely to contain two *Sa*MazF dimers, corresponding to a solvent content of 34.1%. Structure determination is ongoing and is likely to increase our understanding of MazF-mediated mRNA degradation.

This work was supported by NIH grant AI076298 and by grants from FWO, OZR-VUB and VIB. The authors thank Andrew Thompson for beamline support.

References

Amitai, S., Kolodkin-Gal, I., Hananya-Meltabashi, M., Sacher, A. & Engelberg-Kulka, H. (2009). *PLoS Genet.* **5**, e1000390.

Amitai, S., Yassin, Y. & Engelberg-Kulka, H. (2004). *J. Bacteriol.* **186**, 8295–8300.

Baik, S., Inoue, K., Ouyang, M. & Inouye, M. (2009). *J. Bacteriol.* **191**, 6157–6166.

Bravo, A., de Torrontegui, G. & Díaz, R. (1987). *Mol. Gen. Genet.* **210**, 101–110.

Buts, L., Lah, J., Dao-Thi, M.-H., Wyns, L. & Loris, R. (2005). *Trends Biochem. Sci.* **30**, 672–679.

Christensen-Dalsgaard, M. & Gerdes, K. (2008). *Nucleic Acids Res.* **36**, 6472–6481.

Collaborative Computational Project, Number 4 (1994). *Acta Cryst.* D**50**, 760–763.

Donegan, N. P. & Cheung, A. L. (2009). *J. Bacteriol.* **191**, 2795–2805.

Fu, Z., Donegan, N. P., Memmi, G. & Cheung, A. L. (2007). *J. Bacteriol.* **189**, 8871–8879.

Gerdes, K., Christensen, S. K. & Løbner-Olesen, A. (2005). *Nature Rev. Microbiol.* **3**, 371–382.

Gerdes, K., Rasmussen, P. B. & Molin, S. (1986). *Proc. Natl Acad. Sci. USA*, **83**, 3116–3120.

Inouye, M. (2006). *J. Cell. Physiol.* **209**, 670–676.

Kolodkin-Gal, I., Hazan, R., Gaathon, A., Carmeli, S. & Engelberg-Kulka, H. (2007). *Science*, **318**, 652–655.

Lehnherr, H., Maguin, E., Jafri, S. & Yarmolinsky, M. B. (1993). *J. Mol. Biol.* **233**, 414–428.

Li, G.-Y., Zhang, Y., Chan, M. C., Mal, T. K., Hoeflich, K. P., Inouye, M. & Ikura, M. (2006). *J. Mol. Biol.* **357**, 139–150.

Magnuson, R. D. (2007). *J. Bacteriol.* **189**, 6089–6092.

Ogura, T. & Hiraga, S. (1983). *Proc. Natl Acad. Sci. USA*, **80**, 4784–4788.

Otwinowski, Z. & Minor, W. (1997). *Methods Enzymol.* **276**, 307–326.

Pandey, D. P. & Gerdes, K. (2005). *Nucleic Acids Res.* **33**, 966–976.

Suzuki, M., Zhang, J., Liu, M., Woychik, N. A. & Inouye, M. (2005). *Mol. Cell*, **18**, 253–261.

Van Melderen, L. (2010). *Curr. Opin. Microbiol.* **13**, 781–785.

Yamaguchi, Y. & Inouye, M. (2009). *Prog. Mol. Biol. Transl. Sci.* **85**, 467–500.

Zhang, Y., Zhang, J., Hoeflich, K. P., Ikura, M., Qing, G. & Inouye, M. (2003). *Mol. Cell*, **12**, 913–923.

Zhu, L., Inoue, K., Yoshizumi, S., Kobayashi, H., Zhang, Y., Ouyang, M., Kato, F., Sugai, M. & Inouye, M. (2009). *J. Bacteriol.* **191**, 3248–3255.